# Hydroxypropyl Cellulose films Filled with Halloysite Nanotubes/Wax hybrid microspheres

Lorenzo Lisuzzo[a], Maria Rita Caruso[a,b], Giuseppe Cavallaro[a,b], Stefana Milioto[a,b], Giuseppe Lazzara[a,b]

[a]Dipartimento di Fisica e Chimica, Università degli Studi di Palermo, Viale delle Scienze, pad. 17, 90128 Palermo, Italy. *giuseppe.lazzara@unipa.it*

[b]Consorzio Interuniversitario Nazionale per la Scienza e Tecnologia dei Materiali, INSTM, Via G. Giusti, 9, I-50121 Firenze, Italy

**Keywords**: Halloysite nanotubes, wax, bioplastics, biopolymer, nanocomposites.

## Abstract

The design of novel nanocomposite films based on hydroxypropyl cellulose (HPC) and wax/halloysite hybrid microspheres has been reported.

In particular, we firstly prepared wax/clay Pickering emulsions which were characterized by thermogravimetric analysis and microscopy. SEM images allowed to have more detailed insights on the nanotubes disposition at the wax/water interface, acting as an outer stabilizing shell. Therefore, the cellulosic biopolymer was added and it was found that HPC enhances the colloidal stability of the particles, preventing their coalescence and sedimentation. The preparation of the composite films was carried out by solvent casting method, which enabled the development of very homogeneous materials. Contact angle and sliding angle measurements showed that the increasing amount of wax/halloysite microparticles into the biopolymeric matrix is responsible for an enhanced hydrophobic nature of the films and, at the same time, it facilitates the rolling process of droplets on the surfaces, thus making the prepared materials promising protective coatings. These findings were also confirmed by the decrease of the vapor permeability of the nanocomposites, which can act as gas barrier. Moreover, the effect of the composition on the optical properties, namely transparency and colorimetric features, was investigated together with the thermal properties of the biofilms. Results demonstrated that the presence of wax/halloysite microspheres as fillers within the HPC matrix has profound effects on the prepared systems, which were evaluated to be good energy storage and heat reservoir materials. In light of these aspects, the new HPC/wax/halloysite nanocomposites represent promising tools for the surface modification.

## 1. Introduction

Cutting-edge technologies have recently acquired a certain importance in order to develop innovative smart functional materials and to tackle some critical technological issues.[1] The creation of a new material strictly depends on the preparation of its constituent building blocks, which can dictate and control the overall features of the resulting engineered architecture.[2,3] Among the wide range of different new platforms that have been prepared and investigated, the design of emulsions is very attractive and it presents many advantages due to the possibility to reach thermodynamic stability.[4] In particular, the versatility of colloidal particles endows the emulsion systems with some unique and tailored features which enable the fabrication of a wide range of different materials.[5,6] It is well-known that an emulsion is a multiphase system composed of two immiscible liquids where one of them is dispersed into the other in the form of droplets.[7] Despite emulsions are usually stabilized by surfactants or amphiphilic species, the interface of a multiphasic system can also be stabilized by interfacially-active solid particles, as firstly reported by the pioneering studies of Ramsden and Pickering.[8,9] In particular, the mechanism of stabilization is referred to a kinetic barrier that avoids the coalescence and agglomeration due to steric hindrance and volume exclusion.[10] Recently, several biopolymers have been employed for the design of Pickering emulsions, and namely polysaccharides and their derivatives,[10–12] macromolecules such as proteins and lipids,[13–16] cellulosic materials such as micro- and nano-fibrils or nanocrystals.[17,18] Besides the ‘‘surfactant-free” character of these systems, Pickering emulsions meet the current demand for green and ecofriendly materials using particles derived from renewable and eco-sustainable sources.[19] A wide variety of inorganic nanoparticles can be used as stabilizers for oil-in-water emulsions: silica,[20,21] magnetite and iron oxide,[22] gold nanoparticles,[23,24] graphene oxide,[25] latex and naturally occurring clays.[26,27] Unlike conventional emulsions stabilized by surfactants, the possibility to provide a physical barrier to the Pickering emulsions can vary as a function of the nanoparticles main peculiarities such as chemistry and morphology.[28] For instance, nanoclays play a major role within this issue, since they can possess different shape, aspect ratio, specific surface area, anisotropic morphology, surface net charge and functional groups.[29] Among them, Halloysite Nanotubes (HNTs) are natural aluminosilicates whose most distinctive characteristic is their typical hollow tubular morphology.[30] This unique feature provides halloysite with two different surfaces.[31] For instance, the external surface of HNTs is composed of silicon oxygen tetrahedron whereas the internal lumen consists of alumina oxygen octahedrons, so that the outer surface is distributed mainly with Si-O-Si groups and the inner surface is composed of Al-OH.[32,33] As a consequence, the former is negatively charged whilst the latter is positively charged in the 2-8 pH range and they can be selectively modified by both electrostatic and covalent functionalization in order to tailor the

nanoclay physico-chemical properties, thus exploiting the different chemistry of the groups each surface is bearing and their different charge.[34–36] Most importantly, the inner volume of the clay can be loaded with active species and biomolecules for storage and delivery purposes.[37–43] Different in vitro and in vivo studies also reported that HNTs are not toxic and they show cyto-compatibility.[44,45] Literature reports the design of Pickering emulsions with halloysite nanotubes as stabilizing components for applications in oil-spill bioremediation,[46,47] storage and growth of bacterial cultures,[48] catalysis and cultural heritage treatment.[49,50] Besides, one of the main use of HNTs is related to the preparation of nanocomposites.[51,52] Within this field, the employ of clay nanotubes and naturally derived biopolymers plays a major role as alternative for the design of eco-friendly materials aimed to replace the petrolchemical-based plastics,[53,54] thus encouraging a more respectful development model. Indeed, literature reports different strategies and it provides different tools for the preparation of biohybrid functional materials, which can be used in a wide range of technological applications due to their overall properties, such as markedly improved mechanical performances.[55–57] For instance, chitosan nanocomposite films with embedded HNTs and alginate in a tablet-like architecture or cellulose nanofibers based composite papers with halloysite and sepiolite were prepared for drug delivery purposes.[58] Also, pectin bionanocomposite films filled with halloysite nanotubes were developed as potential protective materials for food packaging applications.[59] Furthermore HNTs based nanocomposites with cellulosic derivative polymers (e.g. methylcellulose and hydroxypropyl cellulose) were also investigated as promising perspective for several industrial applications.[60,61] In this work, we tried to move a step forwards. Starting from the attained knowledge about Pickering emulsions and bionanocomposites, we tried to prepare a novel biofilm based on a hydroxypropyl cellulose matrix with embedded paraffin wax/halloysite microspheres. The choice of paraffin as inner core of the pickering emulsion possesses a fundamental importance. Due to its thermal properties, the wax can act as an energy storage material. This aspect is strategic for both the preparation of the pickering emulsions with HNTs entrapped at the oil/water interface and for the application of the resulting biofilm as protective material for packaging purposes and restoration and conservation of cultural heritage.

## 2. Experimental

### 2.1. Materials

Halloysite nanotubes, HNTs ($Al_2Si_2O_5(OH)_4 \cdot 2H_2O$) were a gift from I-Minerals Inc, they possess almost 90% of halloysite with about 9.5% of kaolinite and 0.5% of quartz.

Hydroxypropyl cellulose (HPC, Mw = 80 kg $mol^{-1}$) and microcrystalline wax (melting point from 45 to 58 °C) were Sigma-Aldrich products. Calcium Chloride Dihydrate (≥99%) was from Panreac.

### 2.2. Preparation of wax/halloysite Pickering emulsions

At first, water was heated up to 90 °C and wax was added at the concentration of 0.25 wt. % under magnetic stirring. After the complete melting of paraffin, halloysite nanotubes were added 1,5 wt. % to the mixture. At this point, the dispersion was subjected to ultrasounds for 10 minutes and it was stirred at high temperature condition for 30 minutes. Afterwards, the heating system was turned off in order to cool down the sample while stirring. The obtained emulsion was creamy white and stable for one week at room temperature.

### 2.3. Preparation of composite biofilms

Hydroxypropyl cellulose was dissolved in the Pickering emulsions system at the concentrations of 1 wt. %, 2 wt. %, 3 wt. % and magnetically stirred overnight at room temperature. Each solution was poured into a glass Petri dish (6 cm in diameter) and the solvent casting method was carried out at reduced pressure conditions for 48 h in order to form a thin film. The same procedure was applied for the preparation of a thin film of pure HPC previously dispersed in water and magnetically stirred overnight at room temperature. The composition of the composite films is expressed as mass ratio HNT:HPC ($R_{HNT:HPC}$).

### 2.4 Methods

*2.4.1 Optical microscopy*

The optical micrographs were taken with an Optika polarizing microscope at room temperature, and the size distribution was obtained by using ImageJ software.[62]

*2.4.2 Scanning electron miscroscopy (SEM)*

Electron microscopy images have been carried out by using a microscope ESEM FEI QUANTA 200F. Before each experiment, the surface of the sample was coated with gold in argon by means of an Edwards Sputter Coater S150A to avoid charging under electron beam. The measurements

were carried out in high vacuum mode (< 6 × $10^{-4}$Pa) for simultaneous secondary electron; the energy of the beam was 10 kV and the working distance was 10 mm.

*2.4.3 Water contact angle measurements*

Contact angle measurements were performed by means of an optical contact angle apparatus (OCA 20, Data Physics Instruments) equipped with a video measuring system having a high-resolution CCD camera and a high-performance digitizing adapter. SCA 20 software (Data Physics Instruments) was used for data acquisition. Rectangular (1x2 $cm^2$) films were fixed on top of a plane solid support with double-sided tape and kept flat throughout the analysis. The contact angle (ϑ) of water in air was measured by the sessile drop method by gently placing a droplet of 12.0 ± 0.5 µL onto the surface of the film. Temperature was set at 25.0 ± 0.1 °C for the support and the injecting syringe as well. Images were collected 25 times per second, starting from the deposition of the drop to 60 s. The evolution of ϑ, the evaporation kinetics, the volume (V) and the surface area (A) of droplet was monitored using a software-assisted image-processing procedure. A minimum of 2 droplets were examined for each film sample.

*2.4.4 Sliding angle experiments*

The sliding angle indicates the critical angle at which a liquid droplet begins to slide down on an inclined plate. It is a method to characterize the dynamic interaction at the liquid/solid interface. The sliding angle measurement was performed by wooden support handcraft with a hinge that allows us to change the angle (Figure S1).

A Digital Microscope was used for video measuring system having a high-resolution camera and a high-performance digitizing adapter. Rectangular films (1x2 $cm^2$) were fixed on top of a plane solid support with double-sided tape and kept flat throughout the analysis. It was placed a droplet of 12.0 ± 0.5 µL onto the surface of the film with the injecting syringe and the wood support was gently moved upwards until the drop slides. A Java-based image processing program, ImageJ, was used for data acquisition and sliding angle Φ measured.

*2.4.5. Colorimetric analysis*

Colour parameters of films were measured using a colorimeter (NH300 Colorimeter, 3NH Shanghai Co., Ltd.). The device was calibrated using black and white plates. CQCS3 Software was used for data acquisition. Total colour differences ($\Delta E$), $a*$ (red-green), $L*$ (lightness), and $b*$ (yellow-blue) parameters, whiteness Index (WI) and yellowness Index (YI) were measured for each film and compared with a white coloured surface as indicated by the colorimetric parameters of the standard.

*2.4.6. Thermogravimetry*

The thermogravimetric analysis (TGA) were performed using a Q5000 IR apparatus (TA Instruments, New Castle, DE, USA) under the nitrogen flow of 25 $cm^3$ $min^{-1}$ for the sample and 10 $cm^3$ $min^{-1}$ for the balance. The calibration was carried out by means of Curie temperature of standards (nickel, cobalt and their alloys). The weight of each sample was ca. 10 mg and each sample were placed in a platinum pan and heated from room temperature to 900°C with a rate of 20°C $min^{-1}$. The loading of the polymer and the wax was determined from the residual mass at 700°C by considering the water content as reported in the literature.

*2.4.7. Films Transparency*

The experiments were carried out at 25.0 ±0.1 °C by using a Beckman spectrophotometer (model DU-640). An absorption spectrum was determined for each film. The transmission spectrum was obtained as:

$$T\% = 10^{(2-A)} \quad (1)$$

where A is the absorbance. The attenuation coefficient at the wavelength of 700 nm ($K_{700}$ /$mm^{-1}$) for each sample was computed as:

$$K_{700} = A/(2.3 \times D) \quad (2)$$

where A is the absorbance at wavelength of 700 nm and D is the thickness of the rectangular film measured with a micrometer (±$10^{-3}$ mm). It has to be noted that at 700 nm films do not show any adsorption band.

*2.4.8 Thermal imaging experiments*

Thermal imaging analysis was performed using infrared camera (FLIR E6-XT, FLIR Commercial Systems Inc.) with 43.200 (240 × 180) pixel and wide temperature range from -20 °C to 550 °C. Films were heated at a temperature of 170°C with an electric hot plate. The cooling process was studied taking photos of films each 5-10 minutes with the camera from the range 170°C to 25°C. Thermal images were imported and analysed on FLIR Tools®. Average temperature within each film were calculated in an area of ca. 1x1 $cm^2$.

*2.4.9 Water Permeability Analysis*

The water vapour transmission rate (WVTR) is the rate of water vapour permeating through the film. The tests were carried out at temperature 27 ± 2 °C and 30 ± 2% relative humidity using a saturated solution of Calcium Chloride Dihydrate. Circular bottles (25ml, 1,5 cm inner diameter) were used to determine the water vapour permeability of each film. Biofilms were cut into a circular shape whose diameter was larger than the inner diameter of the bottle and they were fixed, by using a modelling paste, on the top of each bottle. Samples were placed in a desiccator which contained a saturated solution of Calcium Chloride Dihydrate. A thermohygrometer was placed inside the equipment to confirm the environmental parameters (Figure S2-S3).

The water transferred through the films, and absorbed by the desiccant, was determined from the weight loss of the bottle after every hour for a 5h period using an electronic weighing balance (0.00001 g accuracy), then it was decided to measure samples after 24h, 4 days, 7 days, 11 days, 14 days, 20 days and 27 days.

The water vapour transmission rate (WVTR) and water vapour permeability (WVP) were calculated as

$$WVTR=(\Delta m/\Delta tA) \quad (3)$$

$$WVP=WVTR(L/\Delta p) \quad (4)$$

where $\Delta m/\Delta t$ is he slope of each line obtained from the weight loss of samples over time (g/h), $A$ is the exposed surface area of the film ($m^2$), $L$ is the thickness of the film (m), and $\Delta p$ is the difference of partial pressure (Pa) between saturation solution at 32% of relative humidity and saturation water vapour pressure at temperature of 27° C.

## 3. Results and discussion

### *3.1 Halloysite/wax Pickering emulsion: the effect of HPC*

Pickering emulsions based on wax in water stabilized by halloysite nanotubes have been prepared at a temperature above the wax melting point and afterwards they were cooled down to room temperature. This strategy, sketched in Figure 1a, allowed us to obtain stable solid wax microparticles surrounded by halloysite nanotubes. In particular, the wax/HNTs Pickering emulsion system imaged by an optical microscope clearly showed the presence of droplets having a well-defined spherical shape with an average droplet size in the order of tens of microns (Figure 1b).

Besides optical micrographs, the morphology of the samples was also investigated by scanning electron microscopy. Figure 1c reports the image with a lower magnification. It is noteworthy that the proposed protocol allowed the preparation of a significant amount of Pickering emulsions, which are perfectly shaped and quite monodispersed in size. The details of the particles external surface are enlighten in Figure 1d. Herein, SEM micrographs with higher magnification clearly show the presence of halloysite nanotubes at the interface. HNTs completely cover the solid wax emulsions and they are preferentially oriented onto the spherical surface, following its proper curvature. This effect is most likely due to the choice of the paraffin as inner core, which forms liquid emulsions at high temperature conditions but it solidifies when cooled down, thus entrapping the inorganic nanotubes at its external surface. Interestingly, the particle distribution was unaltered if the emulsion is dried out at ambient temperature and reduced pressure and re-dispersed in water.

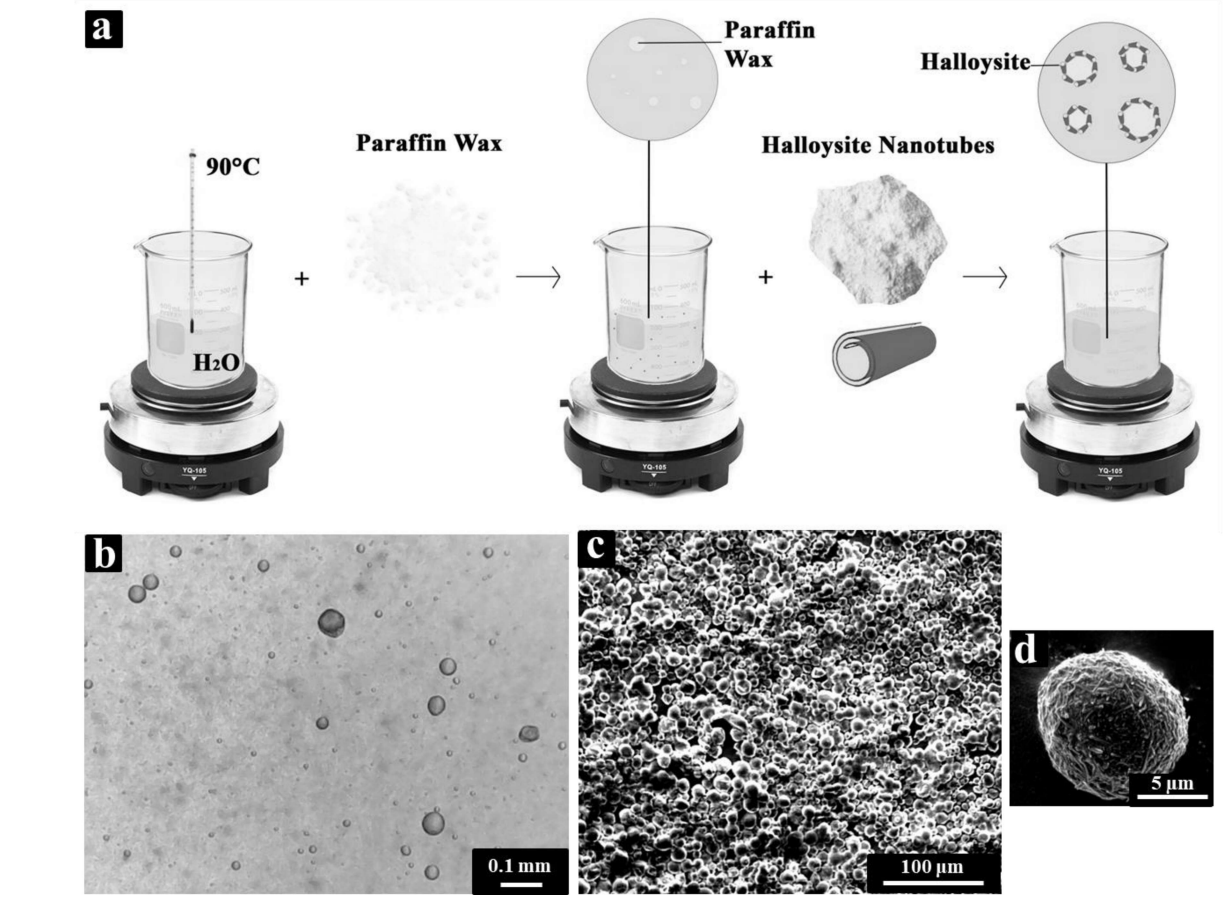


**Figure 1.** Scheme of the preparation protocol (a), optical images (b) and Scanning Electron Microscopy images (c,d) of the halloysite/wax Pickering emulsions.

Then, a stable aliquot of the emulsion was pipetted into a Petri dish and dried out under reduced pressure before thermogravimetric analysis. For comparison, wax and halloysite were also measured. Derivative mass signals (Figure 2) show the wax main degradation between 200 and

300°C while halloysite possesses the typical dehydration mass loss at ca. 500°C.[63] As concerns the wax/halloysite particles the mass losses of both paraffin and clay are evidenced and, by using the rule of mixtures (see SI) taking into account the different water content for each material, one can estimate that the wax represents 3.1% by mass or 8.4% by volume. The relatively large amount of halloysite in the wax/halloysite particles indicates that the nanotubes are not only at the interface but they may penetrate the spherical particle.

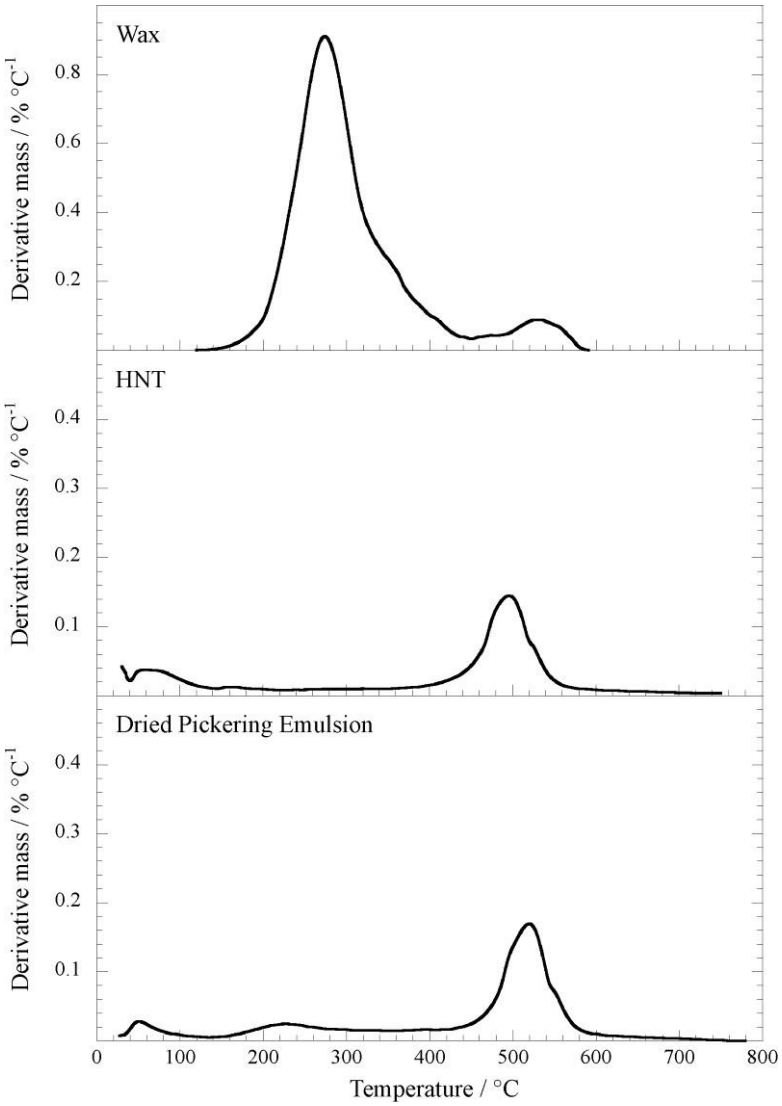


**Figure 2**. Differential thermogravimetric analysis for wax, Halloysite nanotubes and dried wax/halloysite particles.

Literature reports for oil/halloysite based emulsions indicate that adding biopolymers can either stabilize or disrupt the colloidal stability of such a system.[50] With this in mind we prepared the wax/halloysite Pickering emulsions in water and the addition of variable amounts of hydroxypropyl

cellulose (HPC) was tested. From a visual inspection of the emulsion systems, one can conclude that the presence of HPC enhances the colloidal stability over time, thus hindering the particles coalescence and settling (Figure 3).

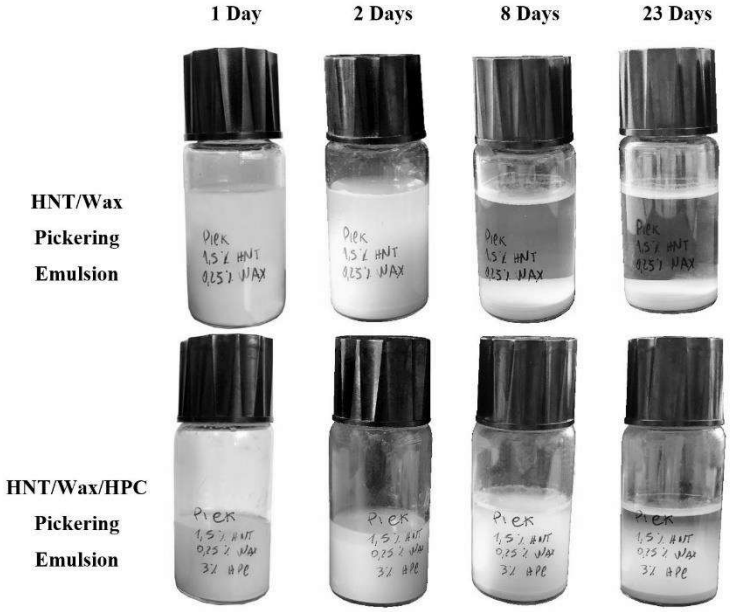


**Figure 3.** Optical images of Pickering emulsions at different time intervals after their preparation.

An example of optical microscopy image for Pickering emulsion containing HPC is provided in Figure 4, where its effect on the particles overall dimensions is also highlighted.

Indeed, HPC influences the droplets size distribution and, in particular, the increase of the polymer amounts is responsible for a smaller drop size. These results are in agreement with the stabilization of the emulsions observed in Figure 3 and they can be explained by considering the ability of HPC in lowering the surface tension of water. A similar result was observed in the presence of pectin for liquid oil in water Pickering emulsions.[50]

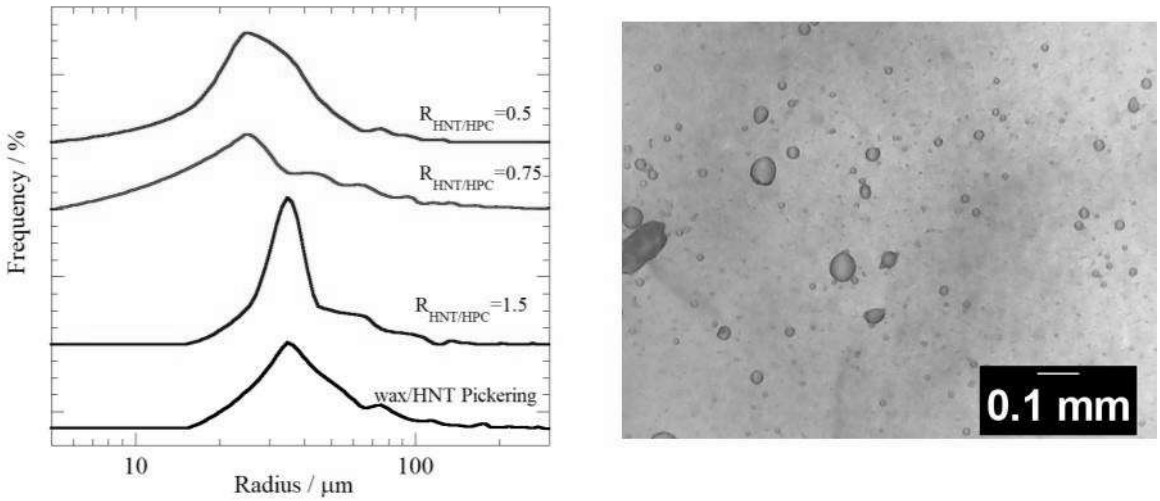


**Figure 4.** Size distribution and optical microscopy image of wax/HNTs Pickering emulsions in the presence of HPC.

### *3.2 Composite biofilms*

Thereafter, nanocomposites based on wax/halloysite particles containing variable amounts of HPC were prepared. The film forming ability of HPC is well documented in literature;[60] the presence of wax in such a polymer matrix can tune the physico-chemical properties. The optical microscopy images of the prepared films are provided in Figure 5 and they are very homogeneous, with the only exception of the sample containing the largest amount of wax/halloysite particles that clearly shows different domains within the system.

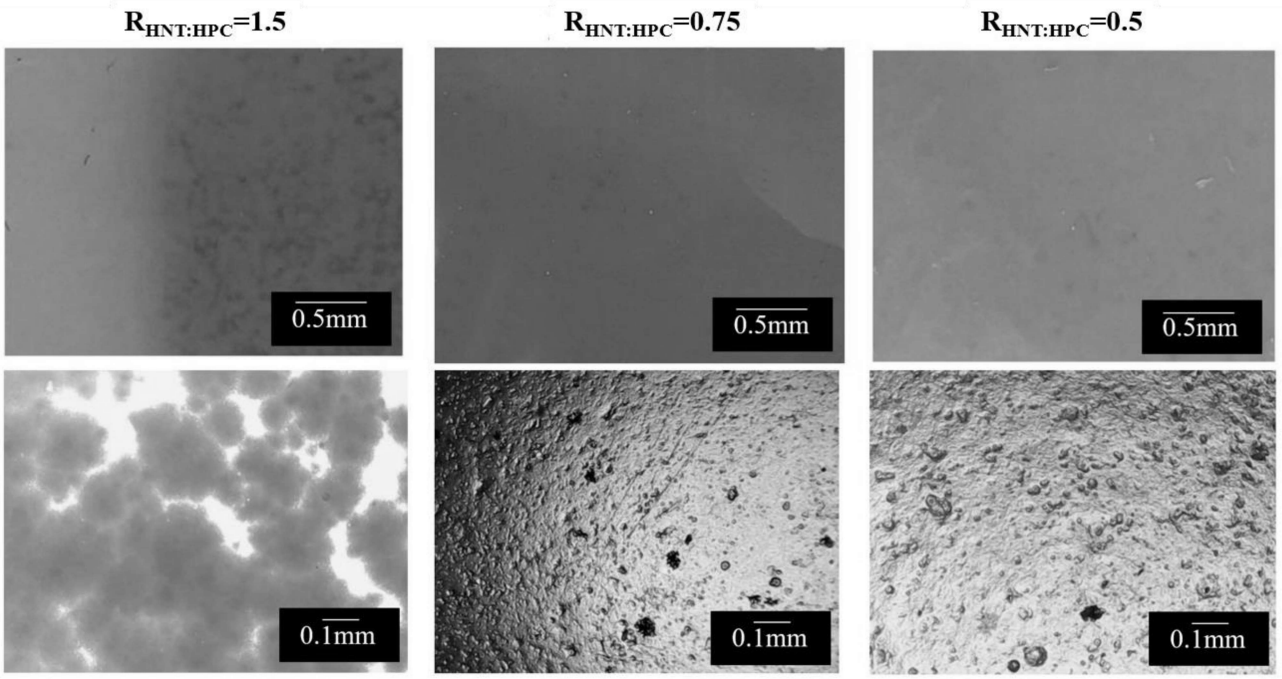

**Figure 5.** Optical images of HPC films containing wax/halloysite particles. Bottom images have been collected under transmitted light.

*3.2.1 Water contact angle and sliding angle*

As a matter of fact, the key factors influencing the surface wettability of a material are: i) the chemical composition and therefore its water affinity; ii) the surface roughness. Therefore, water contact angle ($\vartheta$) and sliding angle ($\Phi$) measurements are sensitive to both these properties and they represent important parameters to provide the suitability of a given film for a specific application. In case of biofilms with a relevant water affinity, the time resolved experiments are needed as the $\vartheta$ values can vary over time due to adsorption/spreading phenomena. The $\vartheta$ vs time curves show an exponential function that can be analyzed quantitatively through the following equation:[64]

$$\vartheta=\vartheta_i \exp(k_\vartheta \tau^n) \quad (5)$$

where ($\vartheta$i) is the zero time extrapolated contact angle, $k_\vartheta$ measures the process rate, and n assumes fractional values ascribable to the occurrence of absorption and spreading mechanisms. Equation successfully fitted our data, providing the parameters reported in Table 1. The n values reveal that both spreading and absorption take place. Accordingly, n = 0 and 1 for pure absorption and pure spreading, respectively.[64]

As evidenced in Figure 6, a higher percentage of HNTs and therefore of wax/halloysite particles causes an increase of $\vartheta$ in agreement with a more hydrophobic nature of the surface. It should be noted that a steady value of contact angle (ca. 90°) is obtained above ca. $R_{HNT:HPC}$=0.3 indicating that the surface saturation is reached and therefore it can not be altered by further addition of paraffin/nanoclay microspheres. It is noteworthy that, from the percolation theory, a value of ≈ 0.3 is expected as a limit for interconnected particles in weekly interacting systems in agreement with the contact angle findings.[65]

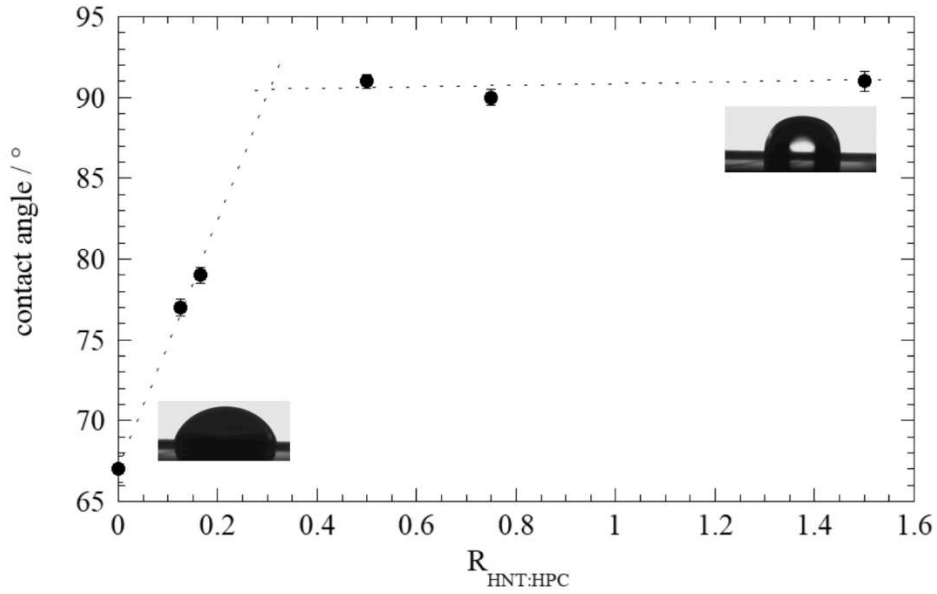


**Figure 6.** Contact Angle extrapolated at zero time for HPC films containing HNT/wax particles.

As concerns the sliding angle, it shows that the droplet rolling process under gravity is facilitated in the presence of the wax/halloysite particles being Φ values lower than that for HPC (see Table 1). Therefore, the cooperation between the low surface energy and the presence of micrometric structures results in a high water contact angle and a small sliding angle. The low values of sliding angles are promising for the film protection ability as it endows a rapid removal of droplets decreasing the possibility of sludge accumulation onto the protected material.

**Table 1.** Water Contact Angle Fitting Parameters and Sliding Angle Values.

| $R_{HNT:HPC}$ | $k_\vartheta/s^{-n}$ | n | Φ / ° |
|---|---|---|---|
| 0 | 0.058 ± 0.008 | 0.299±0.001 | 17.8 |
| 0.125 | 0.032 ± 0.002 | 0.331±0.001 | |
| 0.165 | 0.015 ± 0.005 | 0.534±0.007 | |
| 0.50 | 0.094 ± 0.004 | 0.346±0.004 | 13.5 |
| 0.75 | 0.046 ± 0.006 | 0.370±0.001 | 11.4 |
| 1.50 | 0.056 ± 0.006 | 0.390±0.001 | 8.4 |

*3.2.2 Water Permeability analysis*

The water transport properties through the prepared biofilms have been investigated by measuring the water vapour permeability (Figure 7).

The HPC film containing the wax/halloysite particles have smaller WVP value compared to the pristine polymer. In particular a monotonic decrease of WVP vs $R_{HNT:HPC}$ is observed up to a nearly

constant value. Based on literature such a monotonic decrease in nanocomposites can be ascribed to efficient tortuosity effect and/or decrease of polymer sorption sites.[66] The first contribute is relevant when particles with high aspect ratios are employed while the second contribute reflects the better filler/matrix affinity than matrix/transported molecule. In our case, the filler has a spherical symmetry and therefore the second term should be the dominant one.

It should be noted that the abrupt change in WVP vs $R_{HNT:HPC}$ is consistent with the water contact angle results and therefore with the percolation limit of the system.

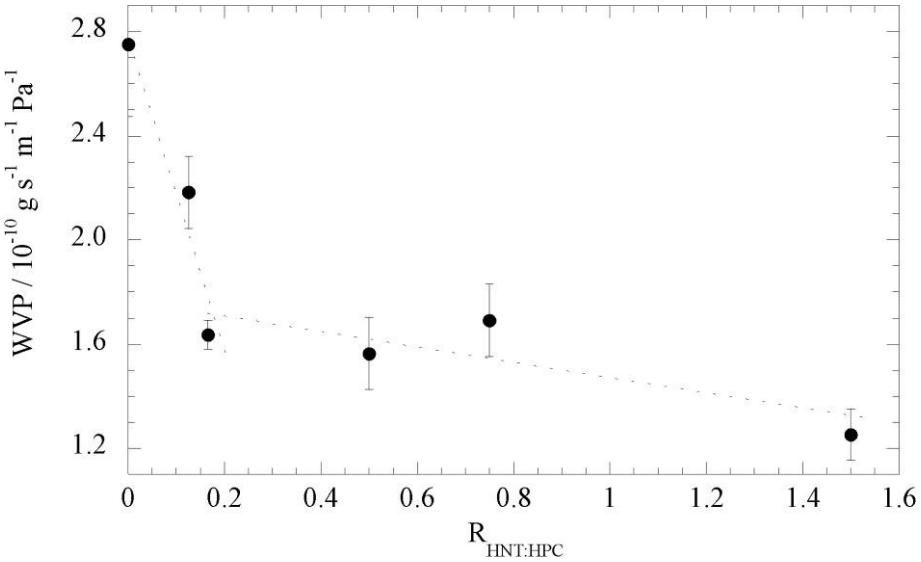


**Figure 7**. Water vapour permeability for HPC films containing variable amount of wax/halloysite particles.

*3.2.3 Optical properties: Colorimetric and Transparency*

Color and transparency of polymeric films represent important optical properties that are relevant in many industrial applications. The morphology of the film and the filler concentration play a major role in influencing the colorimetric analysis and the efficiency of light scattering for transparency measurement. Both these parameters are sensitive to the presence of fillers. The linear attenuation coefficient is the ability of a material to attenuate the beam of radiation that passes through it due to its density, therefore morphology and the tendency to form aggregates is affected. For all of the investigated systems, the light attenuation coefficient values are almost independent from the wavelength in the 400 to 800 nm range (values are reported in Table S1) and therefore the

attenuation coefficient at 700 nm ($K_{700}$) will be discussed hereafter. The $K_{700}$ dependence on the filler concentration for a polymeric films containing spherical particles is:[67]

$$K_{700} \propto \phi R \quad (6)$$

where R is the radius of the spherical particles scattering light while $\phi$ is their volume fraction. The trend in Figure 8 confirms the expected changes in the attenuation coefficient and it proves the good dispersion of the wax/halloysite particles within the polymer matrix up to $R_{HNT:HPC}$=0.75.

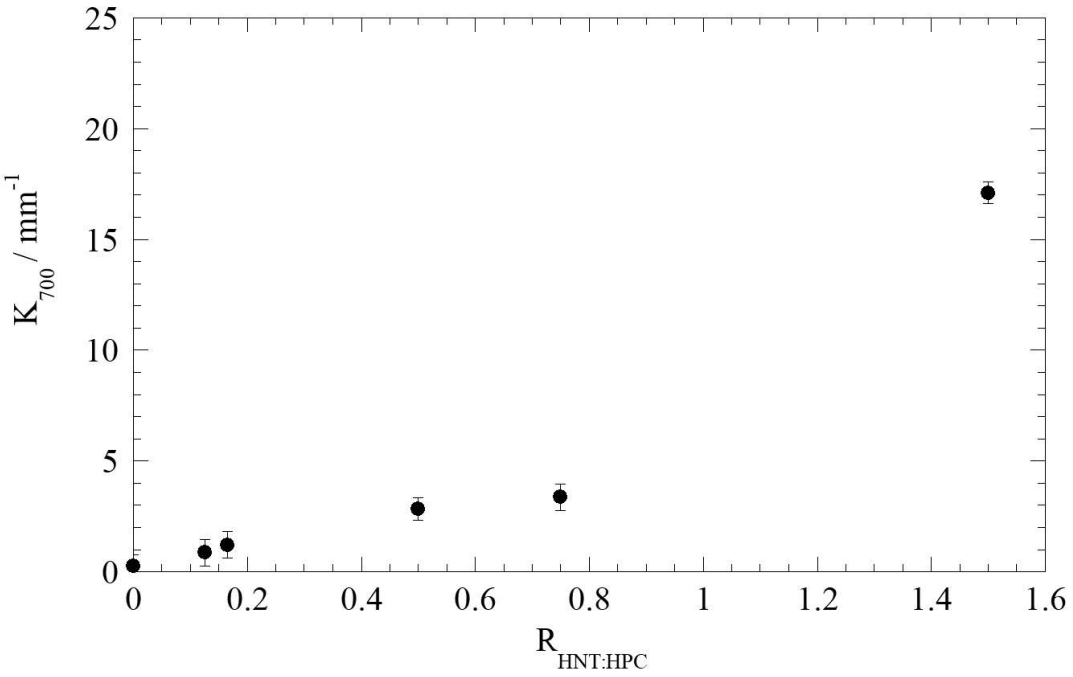


**Figure 8**. Attenuation coefficient at 700 nm for HPC films containing variable amount of wax/halloysite particles.

The colorimetric data of films where collected by placing the film onto a standard white and the results are reported in Table 2. The CIELAB color space is defined by lightness (L*) and hue (a* and b*). In this color space, L* has the value from 0 (black) to 100 (white). a* (redness, greenness) and b* (yellowness and blueness) have positive or negative values to indicate a chromatic color. The color change is calculated with respect to the white standard and expressed as $\Delta E$.[68]

HPC film does not alter the color of the control surface as for human eyes it is reported 2.3 as a $\Delta E$ limit for undistinguished colors.[68]

On the contrary, the lightness L* of films decreased after the addition of wax/halloysite microspheres compared to the control and the chromaticity moves toward yellow as it is well demonstrated in the CIE diagram (Figure 9).

**Table 2**. Colorimetric Parameters.[a]

| $R_{HNT:HPC}$ | L* | a* | b* | ΔE* |
|---|---|---|---|---|
| 0 | 96.37 | -0.26 | 1.71 | 1.685 |
| 0.125 | 91.08 | 1.96 | 14.09 | 15.313 |
| 0.165 | 91.37 | 1.889 | 13.85 | 14.974 |
| 0.5 | 69.47 | 18.30 | 43.82 | 54.911 |
| 0.75 | 71.96 | 16.74 | 42.49 | 52.092 |
| 1.50 | 68.8 | 18.18 | 40.55 | 52.664 |

[a]Control: White Paper, L*=97.166, a*=-0.337, b*=0.224, c*=0.405, h*=146.423

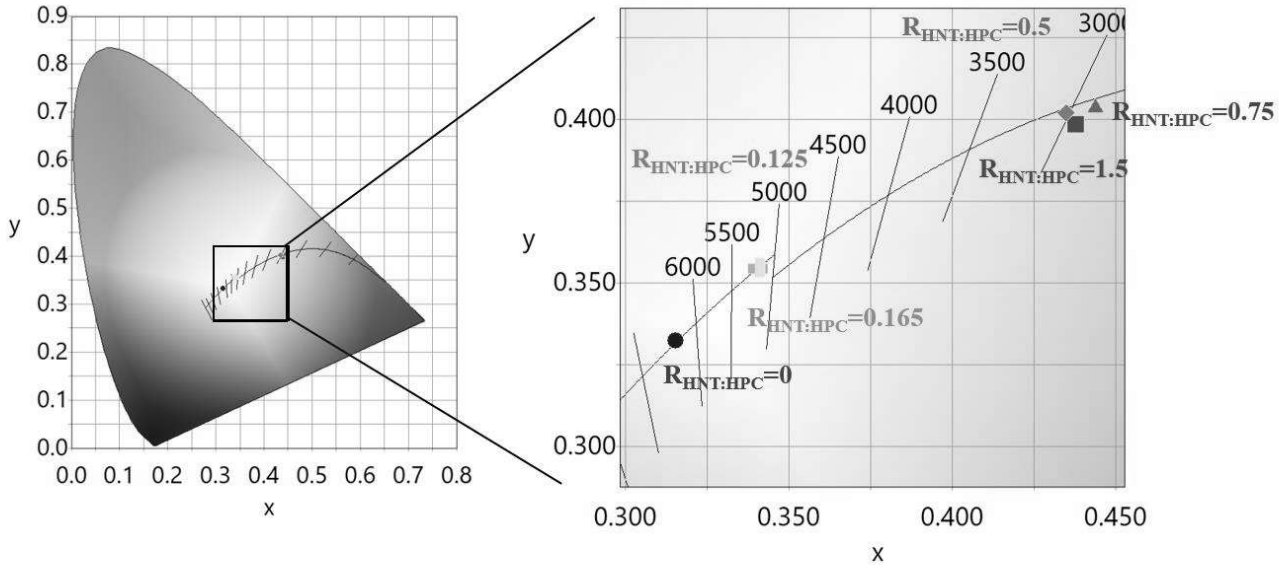


**Figure 9.** Colour parameter displayed on CIE Diagram 1931 2°.

*3.2.4 Thermal behavior: Thermogravimetry and Thermal imaging experiments*

Figure 10 shows the differential thermogravimetric curves (DTG) for the biofilm deriving from HPC and wax/halloysite particles at different ratios. The analysis of the DTG curves provided a clear description of the several degradation steps occurring in the nanocomposites.

The first mass loss occurs in the temperature range between 25 and 150 °C as a consequence of the evaporation of the water physically adsorbed on the materials; the second mass loss (200 - 400°C) is the HPC pyrolytic degradation while the third mass loss above 420°C is due to the two water molecules that are present in the halloysite interlayer.[63] It is evidenced a decrease of the degradation temperature for HPC by 60°C when the maximum amount of wax/halloysite particles are included in the nanocomposite. A similar effect was observed in literature for HPC filled with halloysite nanotubes at filler content above 30 % by mass, therefore the interactions between HPC and the nanoclay are likely responsible of this thermal behaviour.[69]

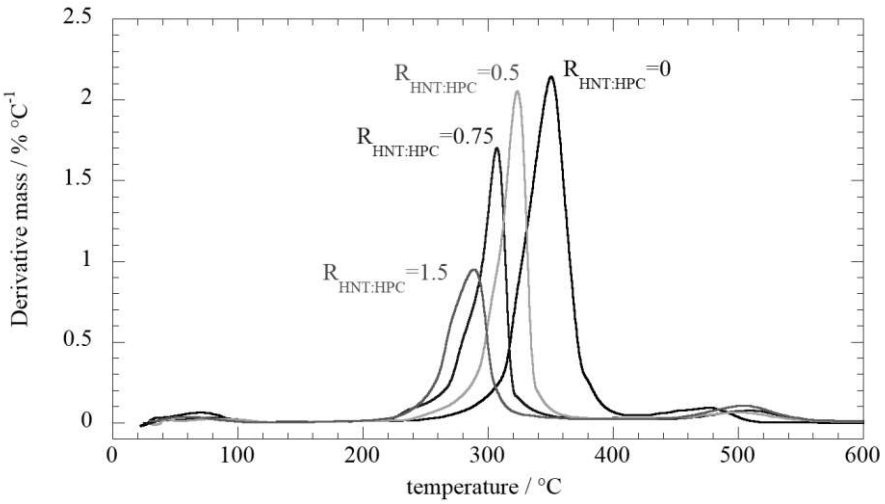


**Figure 10.** Differential thermogravimetric curves for the HPC films containing wax/halloysite particles at variable concentration (full lines).

The dynamic response of the nanocomposites during the cooling was monitored by using a thermocamera and by following the temperature relaxation after heating up the samples onto a hot metal plate at 170 °C (below the degradation temperature observed by TGA). The temperature profiles evidenced an exponential decay following the simple Newton law. The time constant (τ) obtained from the exponential fitting of the experimental temperature vs time data is given by:

$$\tau = \text{mass} \times Cp/(\text{Area} \times HT) \quad (7)$$

where Cp is the specific heat capacity and HT is the heat transfer coefficient of the nanocomposite. Table 3 reports the Cp/HT values obtained after normalization for the mass and the characteristic size of the analyzed materials. The results indicate that the sample with the largest amount of wax/halloysite particles can work as heat reservoir better than pure HPC. This finding is in agreement with other wax/halloysite based composites proposed in the literature.[70]

**Table 3**. Thermal properties from TGA and thermocamera analysis.

| $R_{HNT:HPC}$ | $T_D$ | Cp/HT |
|---|---|---|
| | °C | J $m^2$ $W^{-1}$ $g^{-1}$ |
| 0 | 350.8 | 8.11±0.07 |
| 0.5 | 322.2 | 8.02±0.07 |
| 0.75 | 306.3 | 10.98±0.10 |
| 1.50 | 288.9 | |

## 4. Conclusions

The starting point of this work was the preparation of paraffin based Pickering emulsions with halloysite nanotubes as stabilizing interfacially active solids. The prepared particles were well shaped and quite monodispersed in size, with the inorganic clay covering the external surface and assuming a preferential orientation, as observed by optical and scanning electron microscopies. This effect is probably due to the choice of wax as inner core, which is molten during the preparation procedure and it entraps halloysite upon cooling down due to its transition to the solid state. In particular, we also estimated that that nanotubes can also penetrate the spherical particles, due to their relatively large amount, as investigated by Thermogravimetric Analysis.

Aimed at studying its influence on the stability of the Pickering emulsions, we added variable amounts of hydroxypropyl cellulose (HPC) to the wax/halloysite systems. It was found that HPC enhances the colloidal stability of the particles, avoiding their coalescence thus hindering their aggregation and sedimentation. Therefore, besides the stabilization role of halloysite nanotubes which act as an external steric barrier, the effect of HPC also plays a major role in lowering the surface tension of water, resulting in a very stable system over time.

Then, we moved a step forwards. Indeed, we prepared nanocomposite biofilms by using the solvent casting method, starting from the wax/HNTs Pickering emulsions in presence of the cellulosic polymer. The wettability of the obtained films, which are very homogeneous, was studied by focusing the contact angle and sliding angle. It was found that the former increases as the amount of paraffin/halloysite increases, due to a more hydrophobic nature of the surface, then reaching a constant value at the typical conditions of interconnected particles in weekly interacting systems, according to the percolation theory. For what concerns the sliding angle, instead, the values decrease as the amount of wax/halloysite fillers increases, thus facilitating the rolling process of the droplets on the biofilm surface. This is a very promising factor that enables the system to be used as protecting agent, since it endows an efficient removal of other species from the protected material. Afterwards, water permeability analysis was carried out and it allowed us to demonstrate that the presence of the wax/halloysite spherical particles within the biopolymeric matrix is responsible for a monotonic decrease of the nanocomposites vapor permeability.

Since the optical properties are crucial for many industrial applications, we studied the transparency and colorimetric features of the biofilms. It is noteworthy that both these properties strictly depend on the morphology of the materials and on the filler concentration. For instance, the ability of the prepared samples to attenuate the beam of radiation that passes through them is enhanced by the increasing amount of wax/halloysite fillers within the HPC matrix. Similarly, the chromaticity of the biofilms is affected by the addition of the paraffin/clay microspheres, as demonstrated by the

decrease of the overall lightness. Finally, we investigated the thermal properties of the nanocomposites by focusing their dynamic response upon relaxation after being heated up. This analysis, which was carried out with a thermocamera, allowed us to assess that the prepared films can be used as energy storage and heat reservoir materials. In conclusion, this work reports the preparation of HPC/wax/halloysite biofilms starting from the preparation of paraffin/clay Pickering emulsions. Due to their detailed features, these materials represent an interesting new architecture which can be exploited in many technological application. For instance, findings on wettability, chromaticity, transparency and heat storage efficiency make the prepared biofilms very promising for food packaging and for the protection of surfaces in the field of cultural heritage treatment and conservation.

**Acknowledgments**

The work was financially supported by Progetto di ricerca e sviluppo "AGM for CuHe" (ARS01_00697) and University of Palermo.

## 5. References

(1) Parakhonskiy, B. V.; Parak, W. J.; Volodkin, D.; Skirtach, A. G. Hybrids of Polymeric Capsules, Lipids, and Nanoparticles: Thermodynamics and Temperature Rise at the Nanoscale and Emerging Applications. *Langmuir* **2019**, *35* (26), 8574–8583. https://doi.org/10.1021/acs.langmuir.8b04331.

(2) Sacanna, S.; Korpics, M.; Rodriguez, K.; Colón-Meléndez, L.; Kim, S.-H.; Pine, D. J.; Yi, G.-R. Shaping Colloids for Self-Assembly. *Nature Communications* **2013**, *4* (1), 1688. https://doi.org/10.1038/ncomms2694.

(3) Hueckel, T.; Sacanna, S. Mix-and-Melt Colloidal Engineering. *ACS Nano* **2018**, *12* (4), 3533–3540. https://doi.org/10.1021/acsnano.8b00521.

(4) Yu, L.; Sang, Q.; Dong, M.; Yuan, Y. Effects of Interfacial Tension and Droplet Size on the Plugging Performance of Oil-in-Water Emulsions in Porous Media. *Ind. Eng. Chem. Res.* **2017**, *56* (32), 9237–9246. https://doi.org/10.1021/acs.iecr.7b01770.

(5) Jiang, H.; Sheng, Y.; Ngai, T. Pickering Emulsions: Versatility of Colloidal Particles and Recent Applications. *Current Opinion in Colloid & Interface Science* **2020**, *49*, 1–15. https://doi.org/10.1016/j.cocis.2020.04.010.

(6) Abalymov, A. A.; Parakhonskiy, B. V.; Skirtach, A. G. Colloids-at-Surfaces: Physicochemical Approaches for Facilitating Cell Adhesion on Hybrid Hydrogels. *Colloids and Surfaces A: Physicochemical and Engineering Aspects* **2020**, *603*, 125185. https://doi.org/10.1016/j.colsurfa.2020.125185.

(7) Binks, B. P. Particles as Surfactants—Similarities and Differences. *Current Opinion in Colloid & Interface Science* **2002**, *7* (1), 21–41. https://doi.org/10.1016/S1359-0294(02)00008-0.

(8) Pickering, S. U. CXCVI.-Emulsions. *J. Chem. Soc., Trans.* **1907**, *91* (0), 2001–2021. https://doi.org/10.1039/CT9079102001.

(9) Liu, L.; Hu, Z.; Sui, X.; Guo, J.; Cranston, E. D.; Mao, Z. Effect of Counterion Choice on the Stability of Cellulose Nanocrystal Pickering Emulsions. *Ind. Eng. Chem. Res.* **2018**, *57* (21), 7169–7180. https://doi.org/10.1021/acs.iecr.8b01001.

(10) Sun, H.; Li, S.; Chen, S.; Wang, C.; Liu, D.; Li, X. Antibacterial and Antioxidant Activities of Sodium Starch Octenylsuccinate-Based Pickering Emulsion Films Incorporated with Cinnamon Essential Oil. *International Journal of Biological Macromolecules* **2020**, *159*, 696–703. https://doi.org/10.1016/j.ijbiomac.2020.05.118.

(11) Jiménez-Saelices, C.; Trongsatitkul, T.; Lourdin, D.; Capron, I. Chitin Pickering Emulsion for Oil Inclusion in Composite Films. *Carbohydrate Polymers* **2020**, *242*, 116366. https://doi.org/10.1016/j.carbpol.2020.116366.

(12) Marefati, A.; Wiege, B.; Haase, N. U.; Matos, M.; Rayner, M. Pickering Emulsifiers Based on Hydrophobically Modified Small Granular Starches – Part I: Manufacturing and Physico-Chemical Characterization. *Carbohydrate Polymers* **2017**, *175*, 473–483. https://doi.org/10.1016/j.carbpol.2017.07.044.

(13) Debeli, D. K.; Lin, C.; Mekbib, D. B.; Hu, L.; Deng, J.; Gan, L.; Shan, G. Controlling the Stability and Rheology of Copolyol Dispersions in Fatty Alcohol Ethoxylate (AEO9)-Stabilized Multiple Emulsions. *Ind. Eng. Chem. Res.* **2020**, *59* (40), 18307–18317. https://doi.org/10.1021/acs.iecr.0c03792.

(14) Zafeiri, I.; Smith, P.; Norton, I. T.; Spyropoulos, F. O/W Emulsions Stabilised by Solid Lipid Particles: Understanding How the Particles' Pickering Functionality Can Be Retained Post Their Dehydration and Subsequent Rehydration. *Colloids and Surfaces A: Physicochemical and Engineering Aspects* **2020**, *599*, 124916. https://doi.org/10.1016/j.colsurfa.2020.124916.

(15) Liu, F.; Tang, C.-H. Soy Glycinin as Food-Grade Pickering Stabilizers: Part. I. Structural Characteristics, Emulsifying Properties and Adsorption/Arrangement at Interface. *Food Hydrocolloids* **2016**, *60*, 606–619. https://doi.org/10.1016/j.foodhyd.2015.04.025.

(16) Sarker, M.; Tomczak, N.; Lim, S. Protein Nanocage as a PH-Switchable Pickering Emulsifier. *ACS Appl. Mater. Interfaces* **2017**, *9* (12), 11193–11201. https://doi.org/10.1021/acsami.6b14349.

(17) Silva, C. E. P.; Tam, K. C.; Bernardes, J. S.; Loh, W. Double Stabilization Mechanism of O/W Pickering Emulsions Using Cationic Nanofibrillated Cellulose. *Journal of Colloid and Interface Science* **2020**, *574*, 207–216. https://doi.org/10.1016/j.jcis.2020.04.001.

(18) Zhou, H.; Lv, S.; Liu, J.; Tan, Y.; Muriel Mundo, J. L.; Bai, L.; Rojas, O. J.; McClements, D. J. Modulation of Physicochemical Characteristics of Pickering Emulsions: Utilization of Nanocellulose- and Nanochitin-Coated Lipid Droplet Blends. *J. Agric. Food Chem.* **2020**, *68* (2), 603–611. https://doi.org/10.1021/acs.jafc.9b06846.

(19) Liu, R.; Lu, Y.; Pu, W.; Lian, K.; Sun, L.; Du, D.; Song, Y.; Sheng, J. J. Low-Energy Emulsification of Oil-in-Water Emulsions with Self-Regulating Mobility via a Nanoparticle Surfactant. *Ind. Eng. Chem. Res.* **2020**, *59* (41), 18396–18411. https://doi.org/10.1021/acs.iecr.0c03153.

(20) Koroleva, M.; Bidanov, D.; Yurtov, E. Emulsions Stabilized with Mixed SiO2 and Fe3O4 Nanoparticles: Mechanisms of Stabilization and Long-Term Stability. *Phys. Chem. Chem. Phys.* **2019**, *21* (3), 1536–1545. https://doi.org/10.1039/C8CP05292A.

(21) Koroleva, M. Yu.; Bydanov, D. A.; Palamarchuk, K. V.; Yurtov, E. V. Stabilization of Oil-in-Water Emulsions with SiO2 and Fe3O4 Nanoparticles. *Colloid J* **2018**, *80* (3), 282–289. https://doi.org/10.1134/S1061933X18030080.

(22) Bollhorst, T.; Shahabi, S.; Wörz, K.; Petters, C.; Dringen, R.; Maas, M.; Rezwan, K. Bifunctional Submicron Colloidosomes Coassembled from Fluorescent and Superparamagnetic Nanoparticles. *Angewandte Chemie International Edition* **2015**, *54* (1), 118–123. https://doi.org/10.1002/anie.201408515.

(23) Kosmella, S.; Klemke, B.; Häusler, I.; Koetz, J. From Gel-like Pickering Emulsions to Highly Ordered Superparamagnetic Magnetite Aggregates with Embedded Gold Nanoparticles. *Colloids and Surfaces A: Physicochemical and Engineering Aspects* **2019**, *570*, 331–338. https://doi.org/10.1016/j.colsurfa.2019.03.017.

(24) Yamanaka, K.; Nishino, S.; Naoe, K.; Imai, M. Preparation of Highly Uniform Pickering Emulsions by Mercaptocarboxylated Gold Nanoparticles. *Colloids and Surfaces A: Physicochemical and Engineering Aspects* **2013**, *436*, 18–25. https://doi.org/10.1016/j.colsurfa.2013.06.001.

(25) He, Y.; Wu, F.; Sun, X.; Li, R.; Guo, Y.; Li, C.; Zhang, L.; Xing, F.; Wang, W.; Gao, J. Factors That Affect Pickering Emulsions Stabilized by Graphene Oxide. *ACS Appl. Mater. Interfaces* **2013**, *5* (11), 4843–4855. https://doi.org/10.1021/am400582n.

(26) Abend, S.; Bonnke, N.; Gutschner, U.; Lagaly, G. Stabilization of Emulsions by Heterocoagulation of Clay Minerals and Layered Double Hydroxides. *Colloid Polym Sci* **1998**, *276* (8), 730–737. https://doi.org/10.1007/s003960050303.

(27) Brunier, B.; Sheibat-Othman, N.; Chniguir, M.; Chevalier, Y.; Bourgeat-Lami, E. Investigation of Four Different Laponite Clays as Stabilizers in Pickering Emulsion Polymerization. *Langmuir* **2016**, *32* (24), 6046–6057. https://doi.org/10.1021/acs.langmuir.6b01080.

(28) Calabrese, V.; Courtenay, J. C.; Edler, K. J.; Scott, J. L. Pickering Emulsions Stabilized by Naturally Derived or Biodegradable Particles. *Current Opinion in Green and Sustainable Chemistry* **2018**, *12*, 83–90. https://doi.org/10.1016/j.cogsc.2018.07.002.

(29) Shin, J.; Park, J.; Kim, H. Clay-Polystyrene Nanocomposite from Pickering Emulsion Polymerization Stabilized by Vinylsilane-Functionalized Montmorillonite Platelets. *Applied Clay Science* **2019**, *182*, 105288. https://doi.org/10.1016/j.clay.2019.105288.

(30) Lvov, Y. M.; DeVilliers, M. M.; Fakhrullin, R. F. The Application of Halloysite Tubule Nanoclay in Drug Delivery. *Expert Opinion on Drug Delivery* **2016**, *13* (7), 977–986. https://doi.org/10.1517/17425247.2016.1169271.

(31) Song, Y.; Yuan, P.; Du, P.; Deng, L.; Wei, Y.; Liu, D.; Zhong, X.; Zhou, J. A Novel Halloysite–CeOx Nanohybrid for Efficient Arsenic Removal. *Applied Clay Science* **2020**, *186*, 105450. https://doi.org/10.1016/j.clay.2020.105450.

(32) Pasbakhsh, P.; Churchman, G. J.; Keeling, J. L. Characterisation of Properties of Various Halloysites Relevant to Their Use as Nanotubes and Microfibre Fillers. *Appl. Clay Sci.* **2013**, *74*, 47–57. https://doi.org/10.1016/j.clay.2012.06.014.

(33) Taroni, T.; Meroni, D.; Fidecka, K.; Maggioni, D.; Longhi, M.; Ardizzone, S. Halloysite Nanotubes Functionalization with Phosphonic Acids: Role of Surface Charge on Molecule Localization and Reversibility. *Applied Surface Science* **2019**, *486*, 466–473. https://doi.org/10.1016/j.apsusc.2019.04.264.
(34) Liu, M.; Jia, Z.; Liu, F.; Jia, D.; Guo, B. Tailoring the Wettability of Polypropylene Surfaces with Halloysite Nanotubes. *J. Colloid Interf. Sci.* **2010**, *350* (1), 186–193. https://doi.org/doi: 10.1016/j.jcis.2010.06.047.
(35) Chao, C.; Guan, H.; Zhang, J.; Liu, Y.; Zhao, Y.; Zhang, B. Immobilization of Laccase onto Porous Polyvinyl Alcohol/Halloysite Hybrid Beads for Dye Removal. *Water Sci Technol* **2018**, *77* (3), 809–818. https://doi.org/10.2166/wst.2017.594.
(36) Taroni, T.; Cauteruccio, S.; Vago, R.; Franchi, S.; Barbero, N.; Licandro, E.; Ardizzone, S.; Meroni, D. Thiahelicene-Grafted Halloysite Nanotubes: Characterization, Biological Studies and PH Triggered Release. *Applied Surface Science* **2020**, *520*, 146351. https://doi.org/10.1016/j.apsusc.2020.146351.
(37) Liu, F.; Bai, L.; Zhang, H.; Song, H.; Hu, L.; Wu, Y.; Ba, X. Smart H2O2-Responsive Drug Delivery System Made by Halloysite Nanotubes and Carbohydrate Polymers. *ACS Appl Mater Interfaces* **2017**, *9* (37), 31626–31633. https://doi.org/10.1021/acsami.7b10867.
(38) Aguzzi, C.; Cerezo, P.; Viseras, C.; Caramella, C. Use of Clays as Drug Delivery Systems: Possibilities and Limitations. *Applied Clay Science* **2007**, *36* (1), 22–36. https://doi.org/10.1016/j.clay.2006.06.015.
(39) Viseras, C.; Cerezo, P.; Sanchez, R.; Salcedo, I.; Aguzzi, C. Current Challenges in Clay Minerals for Drug Delivery. *Applied Clay Science* **2010**, *48* (3), 291–295. https://doi.org/10.1016/j.clay.2010.01.007.
(40) Lvov, Y. M.; Shchukin, D. G.; Mohwald, H.; Price, R. R. Halloysite Clay Nanotubes for Controlled Release of Protective Agents. *ACS Nano* **2008**, *2* (5), 814–820. https://doi.org/doi: 10.1021/nn800259q.
(41) Luo, P.; Zhao, Y.; Zhang, B.; Liu, J.; Yang, Y.; Liu, J. Study on the Adsorption of Neutral Red from Aqueous Solution onto Halloysite Nanotubes. *Water Res.* **2010**, *44* (5), 1489–1497. https://doi.org/10.1016/j.watres.2009.10.042.
(42) García-Vázquez, R.; Rebitski, E. P.; Viejo, L.; de los Ríos, C.; Darder, M.; García-Frutos, E. M. Clay-Based Hybrids for Controlled Release of 7-Azaindole Derivatives as Neuroprotective Drugs in the Treatment of Alzheimer's Disease. *Applied Clay Science* **2020**, *189*, 105541. https://doi.org/10.1016/j.clay.2020.105541.
(43) Deng, L.; Yuan, P.; Liu, D.; Annabi-Bergaya, F.; Zhou, J.; Chen, F.; Liu, Z. Effects of Microstructure of Clay Minerals, Montmorillonite, Kaolinite and Halloysite, on Their Benzene Adsorption Behaviors. *Applied Clay Science* **2017**, *143*, 184–191. https://doi.org/10.1016/j.clay.2017.03.035.
(44) Fakhrullina, G. I.; Akhatova, F. S.; Lvov, Y. M.; Fakhrullin, R. F. Toxicity of Halloysite Clay Nanotubes in Vivo: A Caenorhabditis Elegans Study. *Environ. Sci.: Nano* **2015**, *2* (1), 54–59. https://doi.org/10.1039/C4EN00135D.
(45) Zhao, X.; Wan, Q.; Fu, X.; Meng, X.; Ou, X.; Zhong, R.; Zhou, Q.; Liu, M. Toxicity Evaluation of One-Dimensional Nanoparticles Using Caenorhabditis Elegans: A Comparative Study of Halloysite Nanotubes and Chitin Nanocrystals. *ACS Sustainable Chem. Eng.* **2019**, *7* (23), 18965–18975. https://doi.org/10.1021/acssuschemeng.9b04365.
(46) Owoseni, O.; Nyankson, E.; Zhang, Y.; Adams, S. J.; He, J.; McPherson, G. L.; Bose, A.; Gupta, R. B.; John, V. T. Release of Surfactant Cargo from Interfacially-Active Halloysite Clay Nanotubes for Oil Spill Remediation. *Langmuir* **2014**, *30* (45), 13533–13541. https://doi.org/10.1021/la503687b.
(47) Panchal, A.; Swientoniewski, L. T.; Omarova, M.; Yu, T.; Zhang, D.; Blake, D. A.; John, V.; Lvov, Y. M. Bacterial Proliferation on Clay Nanotube Pickering Emulsions for Oil Spill Bioremediation. *Colloids and Surfaces B: Biointerfaces* **2018**, *164*, 27–33. https://doi.org/10.1016/j.colsurfb.2018.01.021.
(48) Panchal, A.; Rahman, N.; Konnova, S.; Fakhrullin, R.; Zhang, D.; Blake, D.; John, V.; Ivanov, E.; Lvov, Y. Clay Nanotube Liquid Marbles Enhanced with Inner Biofilm Formation for the Encapsulation and Storage of Bacteria at Room Temperature. *ACS Appl. Nano Mater.* **2020**, *3* (2), 1263–1271. https://doi.org/10.1021/acsanm.9b02033.
(49) von Klitzing, R.; Stehl, D.; Pogrzeba, T.; Schomäcker, R.; Minullina, R.; Panchal, A.; Konnova, S.; Fakhrullin, R.; Koetz, J.; Möhwald, H.; Lvov, Y. Halloysites Stabilized Emulsions for Hydroformylation of Long Chain Olefins. *Advanced Materials Interfaces* **2016**, 1600435-n/a. https://doi.org/10.1002/admi.201600435.
(50) Cavallaro, G.; Milioto, S.; Nigamatzyanova, L.; Akhatova, F.; Fakhrullin, R.; Lazzara, G. Pickering Emulsion Gels Based on Halloysite Nanotubes and Ionic Biopolymers: Properties and Cleaning Action on Marble Surface. *ACS Appl. Nano Mater.* **2019**, *2* (5), 3169–3176. https://doi.org/10.1021/acsanm.9b00487.
(51) Bugatti, V.; Viscusi, G.; Naddeo, C.; Gorrasi, G. Nanocomposites Based on PCL and Halloysite Nanotubes Filled with Lysozyme: Effect of Draw Ratio on the Physical Properties and Release Analysis. *Nanomaterials* **2017**, *7*, 213. https://doi.org/10.3390/nano7080213.
(52) Gorrasi, G. Dispersion of Halloysite Loaded with Natural Antimicrobials into Pectins: Characterization and Controlled Release Analysis. *Carbohydrate Polymers* **2015**, *127*, 47–53. https://doi.org/10.1016/j.carbpol.2015.03.050.
(53) Takahara, A.; Higaki, Y. Design and Physicochemical Characterization of Novel Organic-Inorganic Hybrids from Natural Aluminosilicate Nanotubes. *RSC Smart Materials* **2017**, No. 22, 131–156. https://doi.org/10.1039/9781782626725-00131.

(54) Bertolino, V.; Cavallaro, G.; Lazzara, G.; Milioto, S.; Parisi, F. Halloysite Nanotubes Sandwiched between Chitosan Layers: Novel Bionanocomposites with Multilayer Structures. *New J. Chem.* **2018**, *42* (11), 8384–8390. https://doi.org/10.1039/C8NJ01161C.

(55) Lisuzzo, L.; Cavallaro, G.; Milioto, S.; Lazzara, G. Effects of Halloysite Content on the Thermo-Mechanical Performances of Composite Bioplastics. *Applied Clay Science* **2020**, *185*, 105416. https://doi.org/10.1016/j.clay.2019.105416.

(56) Liu, M.; Zhang, Y.; Wu, C.; Xiong, S.; Zhou, C. Chitosan/Halloysite Nanotubes Bionanocomposites: Structure, Mechanical Properties and Biocompatibility. *International Journal of Biological Macromolecules* **2012**, *51* (4), 566–575. https://doi.org/10.1016/j.ijbiomac.2012.06.022.

(57) Cheng, C.; Song, W.; Zhao, Q.; Zhang, H. Halloysite Nanotubes in Polymer Science: Purification, Characterization, Modification and Applications. *Nanotechnology Reviews* **2020**, *9* (1), 323–344. https://doi.org/10.1515/ntrev-2020-0024.

(58) Lisuzzo, L.; Cavallaro, G.; Milioto, S.; Lazzara, G. Layered Composite Based on Halloysite and Natural Polymers: A Carrier for the PH Controlled Release of Drugs. *New J. Chem.* **2019**, *43* (27), 10887–10893. https://doi.org/10.1039/C9NJ02565K.

(59) Makaremi, M.; Pasbakhsh, P.; Cavallaro, G.; Lazzara, G.; Aw, Y. K.; Lee, S. M.; Milioto, S. Effect of Morphology and Size of Halloysite Nanotubes on Functional Pectin Bionanocomposites for Food Packaging Applications. *ACS Appl. Mater. Interfaces* **2017**, *9* (20), 17476–17488. https://doi.org/10.1021/acsami.7b04297.

(60) Bertolino, V.; Cavallaro, G.; Lazzara, G.; Merli, M.; Milioto, S.; Parisi, F.; Sciascia, L. Effect of the Biopolymer Charge and the Nanoclay Morphology on Nanocomposite Materials. *Ind. Eng. Chem. Res.* **2016**, *55* (27), 7373–7380. https://doi.org/10.1021/acs.iecr.6b01816.

(61) Huang, B.; Liu, M.; Zhou, C. Cellulose–Halloysite Nanotube Composite Hydrogels for Curcumin Delivery. *Cellulose* **2017**, *24* (7), 2861–2875. https://doi.org/10.1007/s10570-017-1316-8.

(62) Rueden, C. T.; Schindelin, J.; Hiner, M. C.; DeZonia, B. E.; Walter, A. E.; Arena, E. T.; Eliceiri, K. W. ImageJ2: ImageJ for the next Generation of Scientific Image Data. *BMC Bioinformatics* **2017**, *18* (1), 529. https://doi.org/10.1186/s12859-017-1934-z.

(63) Lisuzzo, L.; Cavallaro, G.; Pasbakhsh, P.; Milioto, S.; Lazzara, G. Why Does Vacuum Drive to the Loading of Halloysite Nanotubes? The Key Role of Water Confinement. *Journal of Colloid and Interface Science* **2019**, *547*, 361–369. https://doi.org/10.1016/j.jcis.2019.04.012.

(64) Farris, S.; Introzzi, L.; Biagioni, P.; Holz, T.; Schiraldi, A.; Piergiovanni, L. Wetting of Biopolymer Coatings: Contact Angle Kinetics and Image Analysis Investigation. *Langmuir* **2011**, *27* (12), 7563–7574. https://doi.org/doi: 10.1021/la2017006.

(65) Celzard, A.; Pizzi, A.; Fierro, V. Physical Gelation of Water-Borne Thermosetting Resins by Percolation Theory—Urea-Formaldehyde, Melamine-Urea-Formaldehyde, and Melamine-Formaldehyde Resins. *Journal of Polymer Science Part B: Polymer Physics* **2008**, *46* (10), 971–978. https://doi.org/10.1002/polb.21433.

(66) Wolf, C.; Angellier-Coussy, H.; Gontard, N.; Doghieri, F.; Guillard, V. How the Shape of Fillers Affects the Barrier Properties of Polymer/Non-Porous Particles Nanocomposites: A Review. *Journal of Membrane Science* **2018**, *556*, 393–418. https://doi.org/10.1016/j.memsci.2018.03.085.

(67) Pogodina, N.; Cerclé, C.; Avérous, L.; Thomann, R.; Bouquey, M.; Muller, R. Processing and Characterization of Biodegradable Polymer Nanocomposites: Detection of Dispersion State. *Rheologica Acta* **2008**, *47* (5), 543–553. https://doi.org/10.1007/s00397-007-0243-2.

(68) Mokrzycki, W. S.; Tatol, M. Color Difference ΔE : A Survey. *Machine Graphics and Vision* **2011**, No. Vol. 20, No. 4, 383–411.

(69) Cavallaro, G.; Donato, D. I.; Lazzara, G.; Milioto, S. Films of Halloysite Nanotubes Sandwiched between Two Layers of Biopolymer: From the Morphology to the Dielectric, Thermal, Transparency, and Wettability Properties. *J. Phys. Chem. C* **2011**, *115* (42), 20491–20498. https://doi.org/10.1021/jp207261r.

(70) Zhao, Y.; Thapa, S.; Weiss, L.; Lvov, Y. Phase Change Heat Insulation Based on Wax-Clay Nanotube Composites. *Advanced Engineering Materials* **2014**, *16* (11), 1391–1399. https://doi.org/10.1002/adem.201400094.